

Forward-Link Performance of Satellite CDMA With Linear Interference Suppression and One-Step Power Control

Weimin Xiao, *Member, IEEE* and Michael L. Honig, *Fellow, IEEE*

Abstract—Wideband direct-sequence (DS)-code-division multiple-access (CDMA) is a strong candidate for both terrestrial and satellite components of UMTS. The forward-link capacity of a satellite DS-CDMA system with a conventional matched filter (MF) receiver is limited by interference from adjacent beams and possibly overlapping beams from multiple satellites. In this paper, we study the performance of the linear minimum mean squared error (MMSE) receiver for the satellite forward link. System constraints are long propagation delay, which prevents accurate closed-loop power control, and low on-board power consumption, which implies a low received bit energy to noise density ratio at the mobile receiver. We consider a “one-step” power adjustment algorithm which attempts to compensate for random shadowing and path loss, and compare the associated performance of the MMSE and MF receivers. Dual-satellite diversity is also considered. The effect of code rate on performance is studied through the use of punctured convolutional codes and the evaluation of random coding bounds. Our results indicate that linear MMSE interference suppression can improve the quality of service and increase system capacity significantly.

Index Terms—Code-division multiple-access, interference suppression, satellite communications.

I. INTRODUCTION

MANY of the current air interface proposals for third-generation cellular and universal mobile telecommunications systems (UMTSs) are based on wideband direct-sequence (DS)-code-division multiple-access (CDMA) [1]–[3]. CDMA is attractive for the satellite component of UMTS; however, the forward-link capacity may be severely limited by multi-beam interference. Linear minimum mean squared error (MMSE) detection has been proposed for suppression of multiple-access interference in CDMA (e.g., see [4]–[8]), and is appropriate for the forward link, since it does not require knowledge of the spreading codes of the interferers. Here, we study the performance of this technique in the context of a satellite forward-link model. We only consider MMSE performance, ignoring the effects of adaptation, since this gives a benchmark for comparison with the matched filter (MF) receiver.

Manuscript received July 15, 1999; revised June 7, 2001 and January 14, 2002; accepted February 6, 2002. This work was supported in part by the European Space Agency under Contract 12476/97/NL/MV. The editor coordinating the review of this paper and approving it for publication is R. Yates.

W. Xiao was with the Department of Electrical and Computer Engineering, Northwestern University, Evanston, IL 60208 USA. He is now with Motorola Inc., Arlington Heights, IL 60004 USA (e-mail: wxiao1@motorola.com).

M. L. Honig is with the Department of Electrical and Computer Engineering, Northwestern University, Evanston, IL 60208 USA (e-mail: mh@ece.nwu.edu).
Digital Object Identifier 10.1109/TWC.2002.804185

Performance and capacity analyses for satellite CDMA with a conventional MF receiver have been presented in [9]–[12]. Our system model differs from those considered earlier in that it accounts for the antenna gain pattern, log-normal shadowing, inter-beam interference, imperfect power control, and dual-satellite transmit diversity. We do not consider fading due to multipath. Results which are closely related to those presented here are reported in [13]. An important difference, however, is that the model in [13] assumes perfect power control. Also, the analytical approach in [13] is substantially different from our approach, which relies on large system analysis. Additional related work, in which large system analysis is used to evaluate the performance of linear MMSE receivers in other scenarios, is presented in [14]–[16].

The objective of power control is to achieve a target signal-to-interference-plus noise ratio (SINR) at the output of the linear MMSE filter. Previous work on combined power control with the MMSE receiver has been presented in [17] and [18] for a different model than the one considered here. The long propagation delay on a satellite link prevents the use of tight closed-loop power control. Consequently, we study the performance of “one-step” power control, in which the transmitted power is set initially to achieve a target SINR, and is then fixed. The objective is to compensate for the channel attenuation caused by shadowing and path loss. In general, this technique cannot achieve the target SINR since performance also depends on the transmitted powers associated with the other users, and cross correlations and relative delays among the assigned codes [7], [8], [19]. Variability in SINR due to the latter quantities is associated with short spreading codes, which are required by the adaptive algorithms used to minimize mean squared error. Our results indicate, however, that for the forward-link model considered, the residual standard deviation of received power after one-step power control is less than 1 dB.

We also study the performance of multi-satellite reception with different types of transmit diversity combining (i.e., power assignments). There is a tradeoff between the diversity benefit for the desired user in the presence of random shadowing, and the additional interference caused by each additional overlapping beam. Results indicate that selective transmit diversity performs the best, since on average it does not contribute additional interference. Still, other system considerations, such as frequent handoffs may dictate the use of multiple simultaneous transmissions.

Finally, coded performance of linear MMSE detection is studied as a function of code rate. Results are presented for

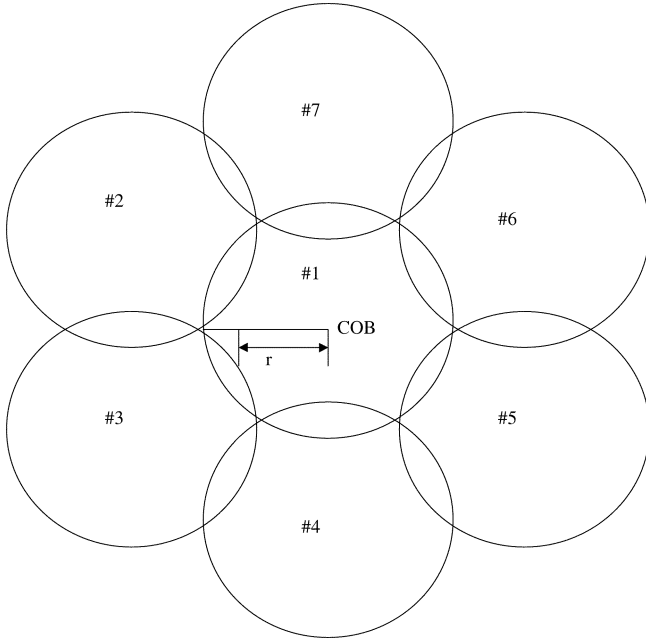


Fig. 1. Satellite beam cluster. “COB” is center of beam.

punctured convolutional codes and corresponding random coding bounds are also evaluated. Results indicate that for the loads considered, the rate 1/2 code performs well for error rates in the range of $10^{-3} - 10^{-4}$.

In the next section, we specify the forward-link satellite model. In Sections III and IV, large system analysis of output SINR with MF and MMSE receivers and one-step power control is presented, based on results in [20]. Satellite diversity is discussed in Section V and uncoded performance comparisons and simulation results are presented in Section VI. Finally, selection of code rate is discussed in Section VII.

II. FORWARD LINK MODEL

A. Notation

For a single satellite, let B denote the number of satellite beams, K denote the number of users per beam (assumed to be the same for each beam), and k_n denote user k in beam n . The geometry of the satellite beams is shown in Fig. 1. The baseband received vector of samples at the output of the chip MF for a particular user, say, user m in beam 1 (m_1), is given by (1) shown at the bottom of the page where $b_k(i)$ is the i th symbol transmitted to user k , $\mathbf{n}_{m_1}(i)$ is the sampled vector for received noise, \mathbf{x}_{m_j} is the location of user m_j , $P^r(k_n \rightarrow \mathbf{x}_{m_j})$ is the received power at location \mathbf{x}_{m_j} due to user k_n , $P_{m_j}^r = P^r(m_j \rightarrow \mathbf{x}_{m_j})$, $h_n(i)$ is

a complex channel coefficient associated with beam n , \mathbf{p}_k is the real-valued spreading code assigned to user k , which repeated each symbol (short code assumption), and \mathbf{p}_k^- and \mathbf{p}_k^+ are the outputs of the chip MF in response to the left- and right-shifted spreading waveform for user k (due to asynchronous beams). All users within each beam are assumed to be synchronized, but random timing offsets are assigned to the different beams. Although our analysis can be applied to chip-asynchronous users across beams, the simulation results assume chip-synchronous transmissions. Multipath is assumed to be negligible, which is typically the case for a satellite link [5]. We also assume perfect phase recovery, and ignore phase variations within each symbol due to high Doppler shifts. (This is considered in [8] and effectively results in complex spreading codes.)

For the forward link, the spreading codes within each beam are orthogonal: $\mathbf{p}_{k_n}^\dagger \mathbf{p}_{l_n} = 0$, $k \neq l$, $n = 1, \dots, B$. These are obtained by masking a random signature sequence (assigned to each beam) with different orthogonal Hadamard codes. Throughout this paper we assume perfect synchronization so that orthogonality among intra-beam codes is maintained at the receiver (mobile unit).

The received power at location \mathbf{x} due to user k_n , $P^r(k_n \rightarrow \mathbf{x})$, depends on the propagation path loss and random shadowing. Let $\Gamma_n(\mathbf{x})$ denote the path loss to location \mathbf{x} associated with beam n , which depends on the antenna pattern, and let $\xi_n(\mathbf{x})$ be a log-normal random variable which models the corresponding random shadowing. The received power at the location of user m_1 due to user k_n is then

$$P^r(k_n \rightarrow \mathbf{x}_{m_1}) = P_{k_n}^t \Gamma_n(\mathbf{x}_{m_1}) \xi_n(\mathbf{x}_{m_1}) \quad \text{for } 1 \leq k \leq K, 1 \leq n \leq B \quad (2)$$

where $P_{k_n}^t$ denotes the transmitted power for user k_n . In what follows, we will ignore correlations in the shadowing random variables among the different users.

The antenna pattern corresponds to an ideal parabolic reflector with gain

$$G(\theta) = \left[J_1 \left(\frac{\pi \left(\frac{D}{\lambda} \right) \sin(\theta)}{\pi \left(\frac{D}{\lambda} \right) \times \sin(\theta)} \right) \right]^2 \quad (3)$$

where θ is the angular offset from the center of the beam, D/λ is the diameter of the antenna divided by the transmission wavelength, and J_1 is the Bessel function of the first kind. For the numerical results in Section VI, we assume that the carrier frequency is 2.19 GHz and $D = 4$ m. As in [7], the beams overlap so that the edge of each beam coincides with a 3-dB loss in the antenna pattern. Fig. 2 shows the antenna gain associated with

$$\begin{aligned} \mathbf{r}_{m_1}(i) = & \sum_{k=1}^K \sqrt{P^r(k_1 \rightarrow \mathbf{x}_{m_1})} h_1(i) \mathbf{p}_{k_1} b_{m_1}(i) \\ & + \sum_{n=2}^B h_n(i) \left\{ \sum_{k=1}^K \sqrt{P^r(k_n \rightarrow \mathbf{x}_{m_1})} [b_{k_n}(i-1) \mathbf{p}_{k_n}^- + b_{k_n}(i) \mathbf{p}_{k_n}^+] \right\} \\ & + \mathbf{n}_{m_1}(i) \end{aligned} \quad (1)$$

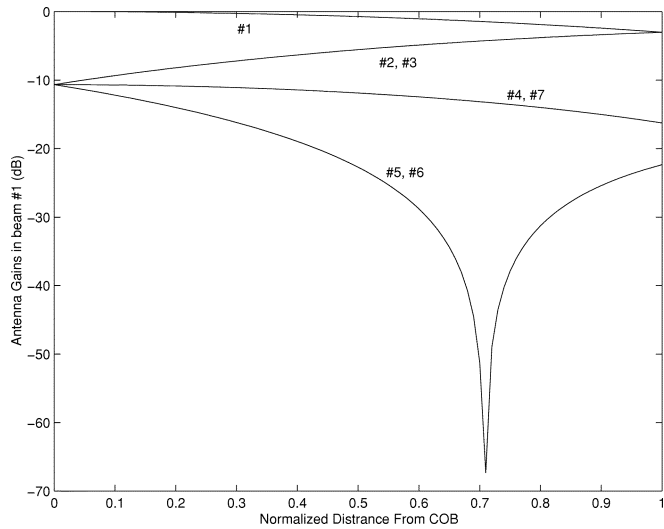


Fig. 2. Antenna gains for each beam.

the seven beams in Fig. 1 as a function of the distance from the center of beam (COB) of beam #1. In the model considered, the performance of users in beam #1 is studied in the presence of interbeam interference from the neighboring six beams.

Our results for dual-diversity assume that a second satellite is present which generates exactly the same configuration of beams from a different orbital position. This is illustrated in Fig. 3. Although this assumption is somewhat unrealistic, it is convenient for analysis and simulation.

B. One-Step Power Control

Because of the long propagation delay in a satellite link, tight iterative power control which enables each user to achieve a performance (SINR) within a narrow range is impractical. For purposes of performance evaluation we consider the following *one-step* power control algorithm.

1. Choose an initial set of transmit powers based on average performance. This average performance is computed off-line, where the average is over the locations of users and shadowing.
2. Measure the output SINR at each receiver.
3. Adjust the transmit powers to achieve a target output SINR assuming all other transmit powers are fixed.

The resulting set of transmit powers gives a distribution of output SINR over the user population. Associated with one-step power control is then an *outage probability*, which is the probability that the output SINR falls below a threshold.

In what follows, we assume that the “desired” users are the users in the center beam #1. To evaluate the effect of other-beam interference on performance, the distribution of transmitted powers after one-step power control is needed. We note that in an infinite array of beams, because of the symmetric distribution for interference power, the transmitted power distribution should be the same within each beam. We

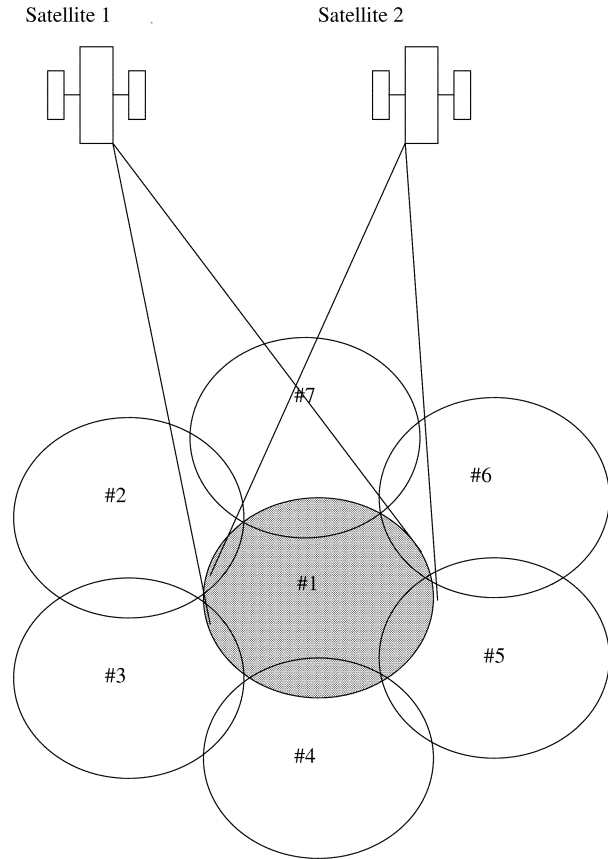


Fig. 3. Beam geometry for dual-satellite system.

will use this observation to obtain the shape of the distribution, and present an iterative method to estimate the total average interference.

III. LARGE SYSTEM PERFORMANCE ANALYSIS

In this section, we apply the large system analysis presented in [20] to approximate the performance of the satellite forward-link model described in the preceding section. The analysis in [20] assumes a synchronous CDMA system with random spreading codes, which is quite different from the model described in the preceding section. Nevertheless, we will see that this type of analysis can still be used to obtain accurate performance estimates. In particular, an infinite-length MMSE receiver in an asynchronous CDMA system gives the same average performance as the MMSE receiver in a synchronous CDMA system [21], [22]. Also, although codes within a beam are orthogonal, the asynchronism among beams and the random outer codes make the random code model a good approximation.¹

The large system limit defined in [20] lets the spreading gain and number of users tend to infinity, i.e., $N, K \rightarrow \infty$, with $K/N = \alpha$ fixed. In what follows, we consider the simple K -user synchronous multiple-access CDMA channel. Let P_k denote the received power of user k , and P denote the received

¹Although the numerical results we present assume a filter that spans a single symbol interval, this gives only a small performance degradation relative to an infinite-length filter. Also, the analytical results obtained are found to be quite close to the simulated results.

power of a random user, which has the limit distribution $F(P)$. It is shown in [20], using results in [23], that the large system limit of the SINR at the output of the MMSE receiver is given by the unique solution to the fixed-point equation

$$\beta_1^* = \frac{P_1}{\sigma^2 + \alpha \int_0^\infty I(P, P_1, \beta_1^*) dF(P)} \quad (4)$$

where σ^2 is the noise variance and

$$I(P, P_1, \beta_1^*) = \frac{P_1 P}{P_1 + P \beta_1^*} \quad (5)$$

is the *effective interference* associated with an interferer received with power P . Note that in the limit, the random variations in SINR over the user population caused by the assignment of random spreading codes disappears. For the MF, the large system limit for SINR is given by

$$\beta_1^* = \frac{P_1}{\sigma^2 + \alpha \int_0^\infty P dF(P)}. \quad (6)$$

To apply these results to the satellite model we first rewrite (4) in terms of the forward-link variables previously defined

$$\beta_{m_1}^* = \frac{P_{m_1}^r}{\sigma^2 + \alpha E\{I[P^r(k_n \rightarrow \mathbf{x}_{m_1}), P_{m_1}^r, \beta_{m_1}^*]\}} \quad (7)$$

where the expectation is with respect to the distribution of $P^r(k_n \rightarrow \mathbf{x}_{m_1})$ over all users k_n .

Let $P_{k_n}^*$ be the target received power for user k_n , i.e., the power that achieves a target SINR based on measured interference plus noise. Then, the corresponding transmitted power for user k_n is

$$P_{k_n}^t = \frac{P_{k_n}^*}{\Gamma_n(\mathbf{x}_{k_n}) \xi_n(\mathbf{x}_{k_n})} \quad (8)$$

and

$$\begin{aligned} P^r(k_n \rightarrow \mathbf{x}_{m_1}) &= P_{k_n}^t \Gamma_n(\mathbf{x}_{m_1}) \xi_n(\mathbf{x}_{m_1}) \\ &= \frac{P_{k_n}^* \Gamma_n(\mathbf{x}_{m_1}) \xi_n(\mathbf{x}_{m_1})}{\Gamma_n(\mathbf{x}_{k_n}) \xi_n(\mathbf{x}_{k_n})}. \end{aligned} \quad (9)$$

Note that $P^r(k_n \rightarrow \mathbf{x}_{m_1})$ depends on $P_{k_n}^*$, the locations of users m_1 and k_n , and the lognormal random variable $\xi_n(\mathbf{x}_{m_1})/\xi_n(\mathbf{x}_{k_n})$. Since $P_{m_1}^r = P_{m_1}^*$ in (7) when $\beta_{m_1}^* = \beta^*$, we conclude that with a fixed σ^2 and target SINR β^* , the target received power for user m_1 , after averaging over the interference as in (7), depends only on the user's location \mathbf{x}_{m_1} and α . We now specify this relation for both the MF and MMSE receivers.

Combining (6) and (9) gives

$$P^*(\mathbf{x}_{m_1}) = \beta_{m_1}^* \left(\sigma^2 + \alpha E_{\mathbf{x}} \left[\frac{P^*(\mathbf{x}_{k_n})}{\Gamma_n(\mathbf{x}_{k_n})} \right] \bar{\Gamma}(\mathbf{x}_{m_1}) \xi \right) \quad (10)$$

where

$$\begin{aligned} \bar{\xi} &= E \left[\begin{array}{c} \xi_1(\mathbf{x}_{k_n}) \\ \xi_k(\mathbf{x}_{k_n}) \end{array} \right] \\ \bar{\Gamma}(\mathbf{x}) &= \frac{1}{B} \sum_{n=2}^B \Gamma_n(\mathbf{x}) \end{aligned}$$

and there is no interference from the desired beam due to the orthogonal inner codes. Multiplying both sides of (10) by $(\Gamma_1(\mathbf{x}_{m_1}))^{-1}$ and taking the expectation over \mathbf{x} gives

$$\begin{aligned} E_{\mathbf{x}} \left[\frac{P^*(\mathbf{x}_{m_1})}{\Gamma_1(\mathbf{x}_{m_1})} \right] &= E_{\mathbf{x}} \left[\frac{1}{\Gamma_1(\mathbf{x}_{m_1})} \right] \\ &\times \beta_{m_1}^* \left\{ \sigma^2 + \alpha \bar{\Gamma}(\mathbf{x}_{m_1}) \bar{\xi} E_{\mathbf{x}} \left[\frac{P^*(\mathbf{x}_{k_n})}{\Gamma_n(\mathbf{x}_{k_n})} \right] \right\}. \end{aligned} \quad (11)$$

Letting $\gamma = E_{\mathbf{x}} [1/\Gamma_n(\mathbf{x})]$, we have $E_{\mathbf{x}} [P^*(\mathbf{x})/\Gamma_n(\mathbf{x})] = \beta_{m_1}^* \sigma^2 \gamma / (1 - \alpha \beta_{m_1}^* \gamma \bar{\xi} \bar{\Gamma}(\mathbf{x}_{m_1}))$. Substituting into (10) gives

$$P^*(\mathbf{x}_{m_1}) = \frac{\sigma^2 \beta_{m_1}^*}{1 - \alpha \beta_{m_1}^* \gamma \bar{\xi} \bar{\Gamma}(\mathbf{x}_{m_1})} \quad (12)$$

where

$$\gamma = E_{\mathbf{x}} [\Gamma_1^{-1}(\mathbf{x})] = 2 \int_0^1 G(r) r dr = 1.4327 \quad (13)$$

\mathbf{x} is assumed to be in beam #1, $G(\theta)$ is given by (3) where $r/H = \tan \theta$ and H is the height of the satellite, and the users are assumed to be uniformly distributed throughout the beam cluster. For the numerical results, r/H is selected so that there is a 3 dB path loss at the edge of the center beam relative to the COB.

It appears to be difficult to obtain a closed-form solution for $P^*(\mathbf{x})$ with the MMSE receiver. One approach is the following iterative method:

$$P_{i+1}^*(\mathbf{x}) = \frac{\beta^* \sigma^2}{1 - \alpha \beta^* E \left[\frac{P^r(k_n \rightarrow \mathbf{x})}{P_i^*(\mathbf{x}) + \beta^* P^r(k_n \rightarrow \mathbf{x})} \right]} \quad (14)$$

where i denotes iteration. The expectation is with respect to location and shadowing, and can be computed by a monte carlo method. Simulations have shown that this iterative method requires few iterations to converge.

IV. ONE-STEP POWER CONTROL

From (12) we see that P^* for the MF depends on \mathbf{x} only through $\bar{\Gamma}(\mathbf{x})$. We observe numerically that $\bar{\Gamma}(\mathbf{x})$ is nearly constant for \mathbf{x} in the center beam, which implies that P^* for the MF receiver is nearly independent of \mathbf{x} . To simplify our model we will make this "location independence" assumption, and sometimes denote P^* as a function of load only, $P^*(\alpha)$. That is, $P^*(\alpha)$ is the received power necessary to achieve a target SINR β^* as a function of load. Additional numerical results indicate that location independence is also an accurate approximation for the MMSE filter. That is, the mean output SINR for the MMSE filter averaged over the locations of other users (assumed to be randomly distributed throughout the seven-beam cluster), code assignments, shadowing, and relative delays among beams is observed to be nearly independent of location. Furthermore, the SINR variance is relatively small at all locations.

For the MMSE receiver, P^* is approximately independent of location since the performance mainly depends on the dimension of the subspace spanned by the strong interferers. For the MF receiver, P^* is approximately independent of location because of the channel model. Namely, the path loss at the edge of each beam is only 3 dB more than at the center and $\bar{\Gamma}(\mathbf{x})$ is nearly constant inside the center beam. This approximation will also be valid for other system models with the MMSE receiver, such as cellular, but is not generally valid with the MF receiver.

The location independent approximation combined with the function $P^*(\alpha)$ enables a relatively simple method for performance evaluation. Substituting the target received power $P^*(\alpha)$ for $P_{m_1}^r$ in (7) gives

$$P^*(\alpha) = \frac{\beta_{m_1}^* \sigma^2}{1 - \alpha \beta_{m_1}^* E \left[\frac{Y}{1 + \beta_{m_1}^* Y} \right]} \quad (15)$$

where

$$Y = \frac{\Gamma_n(\mathbf{x}_{m_1}) \xi_n(\mathbf{x}_{m_1})}{\Gamma_n(\mathbf{x}_{k_n}) \xi_n(\mathbf{x}_{k_n})} \quad (16)$$

and the expectation is with respect to the random location \mathbf{x}_{k_n} and shadowing. Equation (15) will be used to analyze the performance and capacity. This relation suggests the following one-step power control scheme: Compute the target received power as a function of load, as given by (12) or (15), and adjust the transmitted power to compensate for the (measured) shadowing and path loss.

Given a performance target β^* , noise level σ^2 , and the propagation model, the preceding location independence assumption enables us to compute $P^*(\alpha)$. To check the analytical results for finite N , $P^*(\alpha)$ can also be computed off-line using the following iterative method:

- 1) set $P^{*,(0)}(\alpha) = 0$ dB;
- 2) place the users at random locations within the beam cluster;
- 3) compute the path loss and shadowing for each user;
- 4) determine the transmitted power according to (8);
- 5) compute the SINR for user 1, beam #1 (β_{1_1});
- 6) update $P^*(\alpha)$ by adding a correction term,

$$P^{*,(i)}(\alpha) = P^{*,(i-1)}(\alpha) + \mu(\beta_{1_1}^* - \beta_{1_1}^{(i)}) \text{ (dB)} \quad (17)$$

where μ is a constant step-size;

- 7) iterate steps 2–6 until the variations in target received power are sufficiently small.

The step-size μ serves to average over placement of users, code assignments, and delays. Simulations of this iterative method show that several hundred iterations are needed to estimate P^* with $\mu = 0.1$. Numerical results in Section VI show that the fixed points computed by this iterative algorithm are very close to the numerical solution of (15).

Given $P^*(\alpha)$, we compute the transmitted power for user k_n according to the one-step power control scheme

$$P_{k_n}^t = \frac{P^*(\alpha)}{\Gamma_n(\mathbf{x}_{k_n}) \xi_n(\mathbf{x}_{k_n})} \quad (18)$$

where the path loss and shadowing are determined at the mobile and transmitted back to the satellite. Of course, this power control method cannot generally be applied in practice, since α is the combined load of the desired beam and the surrounding beams, and is typically unknown. Furthermore, in a finite system ($N < \infty$), this one-step adjustment does not generally achieve the target SINR due to the random placement of users and the short code assumption [19], [7].

Fig. 4 shows a histogram of the received SINR over the user population after one-step power control obtained from 10^5 runs for both the MF and MMSE receivers. The standard deviation

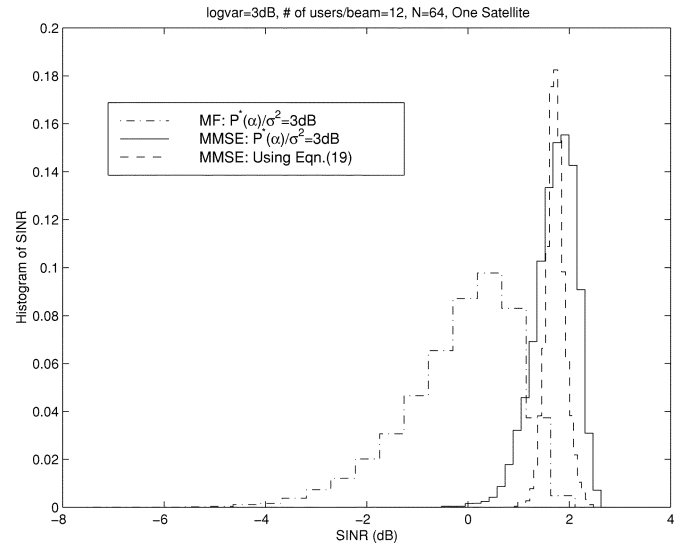


Fig. 4. Histogram of output SINR.

of the shadowing is 3 dB, $P^*(\alpha)/\sigma^2 = 3$ dB, $N = 64$, and there are 12 users per beam. The mean SINRs in the figure are -0.024 dB for the MF and 1.73 dB for the MMSE receiver. The standard deviation for the MMSE receiver (solid line in Fig. 4) is 0.41 dB, which indicates that the one-step power control scheme considered can generally achieve within a narrow range of the target SINR. The histogram shown for the MF assumes long spreading codes, so that random variations due to the random cross correlations are averaged out. The variability in performance shown in Fig. 4 is, therefore, due solely to the random placement of users, which can create a significant power imbalance among received signals. This highlights an important advantage of the MMSE receiver, since it is insensitive to these power variations.

In practice, for both receivers the desired received power can be computed by measuring the received SINR and scaling the transmitted power accordingly. There is a unique solution for β^*/P_k^r in (7) (see [20]) which implies

$$\frac{\beta^*}{P_{m_1}^{t,final}} = \frac{\beta^{init}}{P_{m_1}^{t,init}} \text{ or } P_{m_1}^{t,final} = \frac{P_{m_1}^{t,init} \times \beta^*}{\beta^{init}}. \quad (19)$$

where “init” and “final” refer to the initial and final values of the variable. The expression (19) will be used to obtain numerical results for the single satellite model. Numerical results will also be presented for $P^*(\alpha)$ based on the large system analysis and the location independent approximation.

Of course, this relation trivially achieves the target SINR if only the desired user is allowed to change the transmitted power. If all users change their powers according to the one-step power control scheme, this relation becomes valid only as N and $K \rightarrow \infty$. For finite N , this relation leads to residual variance in the received SINR around the target value, as shown in Fig. 4 (dashed line). The residual standard deviation of SINR is approximately 0.2 dB which is smaller than that obtained using (18). This is because (19) takes into account relative delays and cross correlations among codes, in addition to variations due to path loss and shadowing. Also, (18) introduces some additional variance due to the location independent assumption.

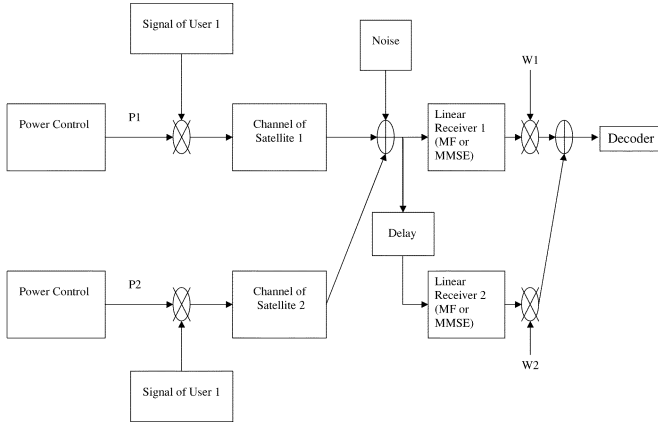


Fig. 5. Dual-satellite diversity with power control.

V. POWER CONTROL WITH DUAL-SATELLITE DIVERSITY

In this section, we discuss one-step power control for the dual-satellite diversity system shown in Fig. 5. The relative delay between the satellites is assumed to be much greater than a symbol, so that within the observation window for each branch, the desired signal from the other satellite acts as independent interference. We assume that coefficients w_1 and w_2 in Fig. 5 are selected to perform maximum ratio combining, so that the output SINR is

$$\beta_{m_1}^* = \beta_{m_1,1} + \beta_{m_1,2} \quad (20)$$

where $\beta_{m_1,1}$ and $\beta_{m_1,2}$ are the SINRs of the two receiver branches and

$$\beta_{m_1,j} = \frac{P_{m_1,j}^r}{\sigma^2 + \alpha E \left[\frac{P_{m_1,j}^r(k_n \rightarrow \mathbf{x}_{m_1}) P_{m_1,j}^r}{P_{m_1,j}^r + \beta_{m_1,j} P_{m_1,j}^r(k_n \rightarrow \mathbf{x}_{m_1})} \right]}, \quad j = 1, 2 \quad (21)$$

where $P_{m_1,j}^r$ is the received power for user m_1 on branch j and $P_{m_1,j}^r(k_n \rightarrow \mathbf{x}_{m_1})$ is the total power received at location \mathbf{x}_{m_1} due to user k_n (summed over independent paths).

The solution for $\beta_{m_1,j}/P_{m_1,j}^r$ in (21) is unique, so that

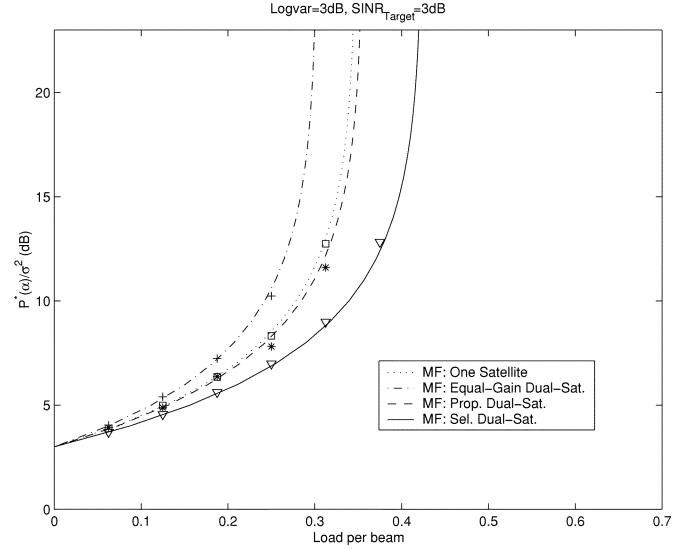
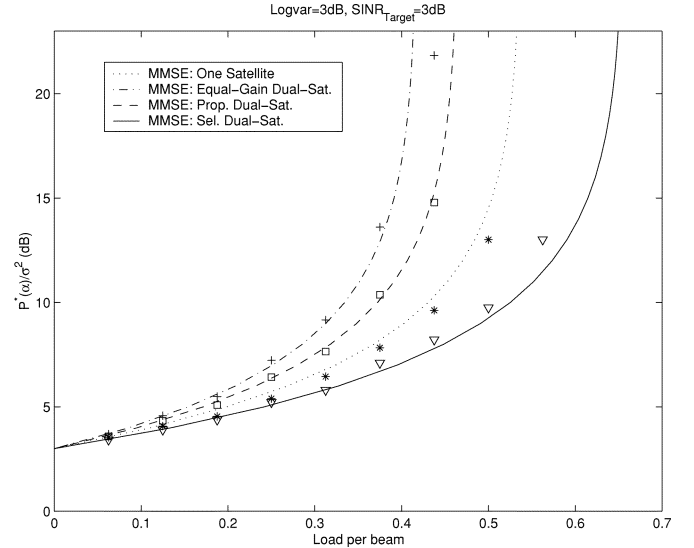
$$\frac{\beta_{m_1,1}}{\beta_{m_1,2}} = \frac{P_{m_1,1}^r}{P_{m_1,2}^r}. \quad (22)$$

Let $P_{m_1}^{sum} = P_{m_1,1}^r + P_{m_1,2}^r$. Substituting $P_{m_1}^{sum}$, (21) and (22) into (20), we get

$$\beta_{m_1}^* = \frac{P_{m_1}^{sum}}{\sigma^2 + \alpha E \left[\frac{P_{m_1}^{sum} P_{m_1}^r(k_n \rightarrow \mathbf{x}_{m_1})}{P_{m_1}^{sum} + \beta_{m_1}^* P_{m_1}^r(k_n \rightarrow \mathbf{x}_{m_1})} \right]} \quad (23)$$

which has the same form as (7). As in the single satellite case, $P_{m_1}^{sum}$ depends weakly on the location of the desired user asymptotically, so that to simplify the analysis we assume that $P_{m_1}^{sum} = P^*(\alpha)$. Note, however, that $P^*(\alpha)$ and the distribution of $P_{m_1}^r(k_n \rightarrow \mathbf{x}_{m_1})$ which appear in the dual-diversity condition (23) are different from the analogous single-satellite quantities. Analogous methods to those described in Section IV can be used to compute $P^*(\alpha)$ for the dual-diversity case.

Numerical results in the next section are shown for three kinds of power assignments: selective, equal-gain, and proportional. Equal gain corresponds to the constraint $P_{m_1,1}^t = P_{m_1,2}^t$ where the superscript t denotes transmitted power. The number of interferers is effectively doubled compared with the single-satellite case. For proportional combining the transmit powers are

Fig. 6. $P^*(\alpha)/\sigma^2$ obtained by solving (15) versus load per beam for the MF receiver. The discrete points correspond to the iterative method in Section IV.Fig. 7. $P^*(\alpha)/\sigma^2$ obtained by solving (15) versus load per beam for the MMSE receiver. The discrete points correspond to the iterative method in Section IV.

proportional to the corresponding propagation gains (analogous to max-ratio combining). The number of interferers is again effectively doubled relative to the single-satellite case. Minimizing the total transmitted power for fixed β^* results in selective transmit diversity, which means that only the satellite corresponding to the strongest received signal transmits. These power assignments apply to both the MF and MMSE receivers. Note that (19) can also be used to adjust powers.

VI. NUMERICAL RESULTS: UNCODED PERFORMANCE

Figs. 6 and 7 show $P^*(\alpha)/\sigma^2$ versus load per beam for the MF and MMSE receivers, respectively. Curves are shown corresponding to the large system analysis and the discrete points correspond to the iterative method in Section IV. The large system analysis accurately predicts the simulation results. The transmitted power depends on the path loss and shadowing according

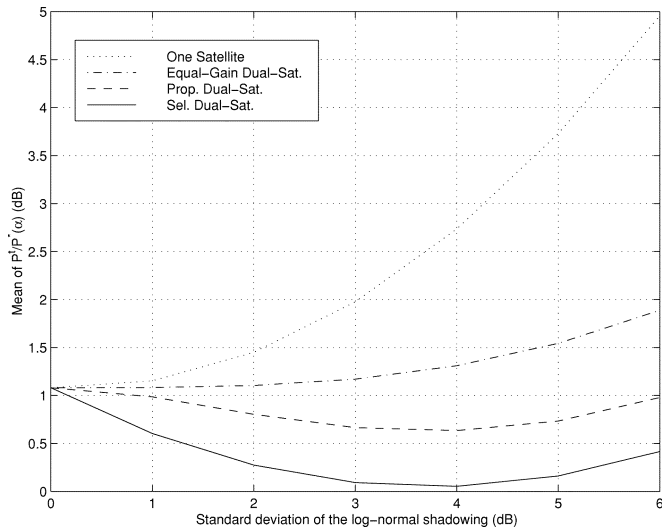


Fig. 8. Relationship between average transmitted power per user and $P^*(\alpha)$.

to (18). Fig. 8 shows the relationship between average transmitted power per user (summed over satellites) and $P^*(\alpha)$. Different plots are shown corresponding to the different power assignment schemes for dual-satellite diversity. These plots apply to both MF and MMSE receivers.

Figs. 6 and 7 show that the MMSE receiver can offer a significant capacity increase relative to the MF receiver, where the gain depends on the total power budget and the type of power assignment used in the dual-diversity case. If the received SNR $P^*(\alpha)/\sigma^2 = 5$ dB, then the gain is between 1.5 and 2 for a 3-dB log-normal standard deviation, and assuming a target SINR of 3 dB. If we fix the load per beam at 0.2, then the gain in received power is between 2 and 3 dB. The relative gain increases with the received power, the load, and the variance of the shadowing. The vertical asymptotes for $P^*(\alpha)/\sigma^2$ shown in the figures correspond to the maximum capacities.

These results show that selective transmit diversity can give a significant improvement in performance relative to the single-satellite case when the variance of shadowing is large. In contrast, although equal and proportional power assignments perform better than the one satellite-case with the MF receiver, they perform somewhat worse than the one satellite case with the MMSE receiver. This difference becomes more pronounced when the variance of the shadowing is small. The reason is again due to the additional interference in the system when two satellites are present.

As explained in Section VI, selective transmit diversity minimizes the total transmitted power and maintains a constant number of interferers on average. This is an important property since the ability of the MMSE receiver to suppress interference depends on the load (ratio of interferers to processing gain). Furthermore, a large load adversely affects the speed of convergence of an adaptive algorithm. Fig. 8 shows that, on average, diversity decreases the transmit power needed to achieve $P^*(\alpha)$. As expected, this savings in power increases with the variance of the shadowing. Combining Figs. 6–8 gives the average transmit power per user needed as a function of load per beam. A practical problem with selection diversity is that switching between satellites is necessary as channel conditions

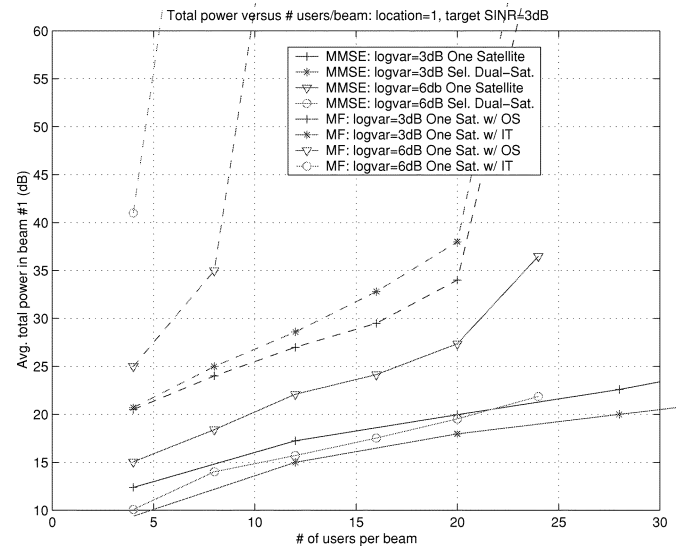


Fig. 9. Average total transmit power per beam $/\sigma^2$ versus number of users per beam. The user is located at the edge of the center beam. The dashed lines correspond to the MF. "IT" refers to iterative power control, and "OS" refers to one-step power control.

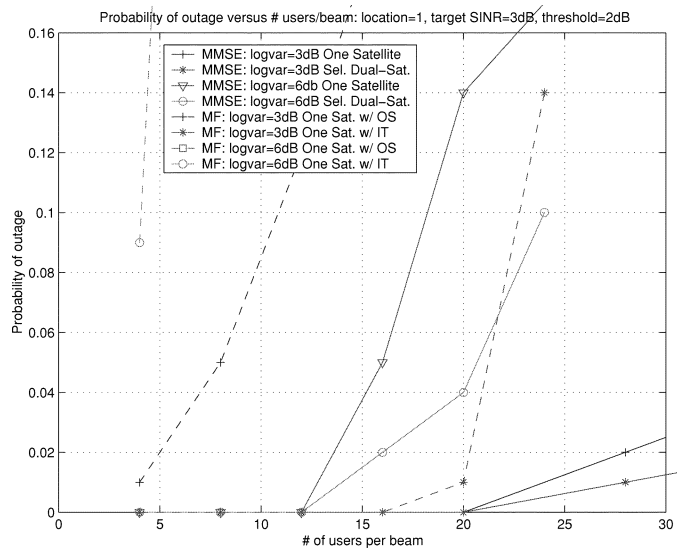


Fig. 10. Outage probability versus number of users per beam. The dashed lines correspond to the MF.

change. In particular, both the shadowing and path loss are time-varying due to the orbital motion of the satellites. The pilot signal, present in each beam, might be used to measure these changes and direct the switching, although frequent handoffs may still necessitate multiple transmissions.

Figs. 9 and 10 show simulated performance results. Fig. 9 shows average total *transmitted* power per beam versus α with one-step power control, and Fig. 10 shows outage probabilities after power control. For these results, the target SINR is 0 dB, the desired user is at the edge of beam #1, and the outage threshold is -1 dB, which means an outage occurs if the output SINR of the desired user after power control is less than -1 dB.

The SINR variability for the MF is quite large, as shown in Fig. 4, so that the outage probability is unacceptably high with one-step power control. Consequently, for the MF, perfect power control is assumed, whereas for the MMSE receiver, (19)

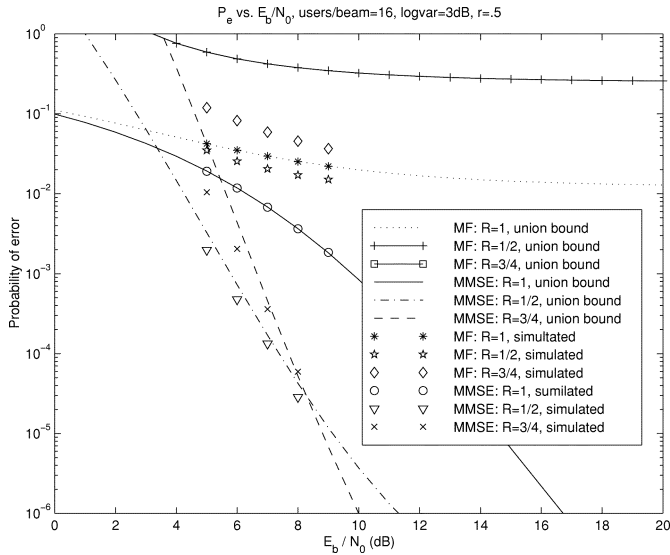


Fig. 11. Error probability versus E_b/N_0 for different code rates.

is used to implement one-step power control. Even with this advantage for the MF, the MMSE receiver with one-step power control can support more than twice the load as the MF receiver and can offer a significant reduction in transmitted power.

With tight, iterative power control Fig. 10 shows that the outage probability of the MF increases sharply after the load per beam crosses a threshold. With one-step power control, the outage probability of the MMSE receiver increases gradually as the number of users increases. Hence, the MMSE filter with one-step power control provides a significantly larger and “softer” capacity. These results also show that selective transmit diversity can offer a moderate increase in capacity relative to a single satellite especially when the variance of shadowing is large.

VII. PERFORMANCE WITH CODING

In this section, we present performance results for a coded system with both MF and MMSE receivers. Throughout this section we assume that the bandwidth expansion (chip rate/information rate) is fixed, so that the number of chips per bit is RN where R is the code rate. For the numerical results, we take $N = 128$. Error probability curves for different code rates are obtained by puncturing the rate 1/2, constraint length 7 convolutional code presented in [24], which has the octal generator matrix [133, 171].

A. Error Probability and Cutoff Rate

Fig. 11 shows error probability versus E_b/N_0 for rate 1/2 and 3/4 codes. The curves were computed from the union bound on error probability, assuming the residual interference plus noise at the output of the receiver filter (MF or MMSE) is Gaussian. Several simulation points are included, which show that the union bound accurately predicts the error probability when it is less than 10^{-3} . In this figure, there are 16 users per beam, the standard deviation of the log-normal shadowing is 3 dB, and the normalized distance of the desired user from the center of beam is $r = 0.5$. With these parameters, the MF receiver is unable to

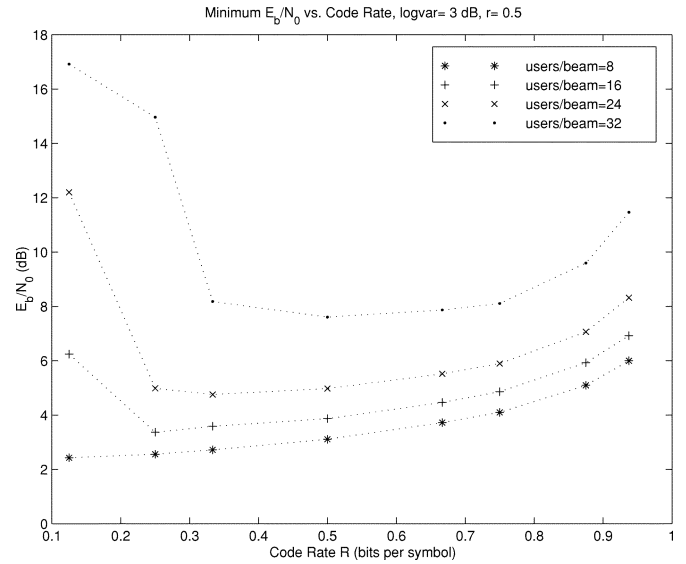


Fig. 12. E_b/N_0 required for reliable communications versus code rate $R = R_0$ for a single satellite. The normalized distance from the COB is 0.5 and the standard deviation of the shadowing is 3 dB.

close the link, i.e., achieve $BER \leq 10^{-3}$. (The union bound for the MF receiver with the rate 3/4 code exceeds one for the range of E_b/N_0 shown.) For the MMSE receiver, the rate 3/4 code performs better than the rate 1/2 code for $E_b/N_0 > 8$ dB. At an error rate of 10^{-6} , the rate 3/4 code gives more than 6-dB coding gain.

We also evaluate the cutoff rate R_0 for the forward-link satellite model. This gives additional insight into selection of code rate, and also gives an upper bound on performance for the codes considered. For a single-user additive white gaussian noise (AWGN) channel, the cutoff rate for binary signaling is [25]

$$R_0 = 1 - \log_2 \left(1 + e^{-E_s/N_0} \right) \quad (24)$$

where $E_s = RE_b$. For a given E_b/N_0 , R_0 is computed by substituting $R = R_0$ and solving the resulting fixed-point condition.

Fig. 12 shows plots of the minimum E_b/N_0 required for reliable communications versus code rate for the forward-link satellite model and for different loads $K/(RN)$. To compute these curves, $E_s/(2N_0)$ in (24) is replaced by the SINR at the output of the MMSE filter. Also, because Hadamard sequences do not exist for all values of RN , the orthogonal spreading sequences within each beam were selected as eigenvectors of a positive definite matrix $\mathbf{S}\mathbf{S}^\dagger$, where the elements of \mathbf{S} are iid ± 1 . The results shown in Fig. 12 were obtained by averaging over the selection of \mathbf{S} (independently chosen for each beam), delays among beams, location of users, and random shadowing.

The interpretation of Fig. 12 is that for a given code rate R , the corresponding E_b/N_0 is the *minimum* E_b/N_0 required to drive the error probability to zero. For a given load, the R for which the corresponding curve is minimized is the optimal code rate in the sense that the E_b/N_0 required to drive the error probability to zero is less than that needed for any other code rate. Fig. 12 shows that, as expected, the optimal code rate generally increases with load and that a rate 1/2 code is nearly optimal

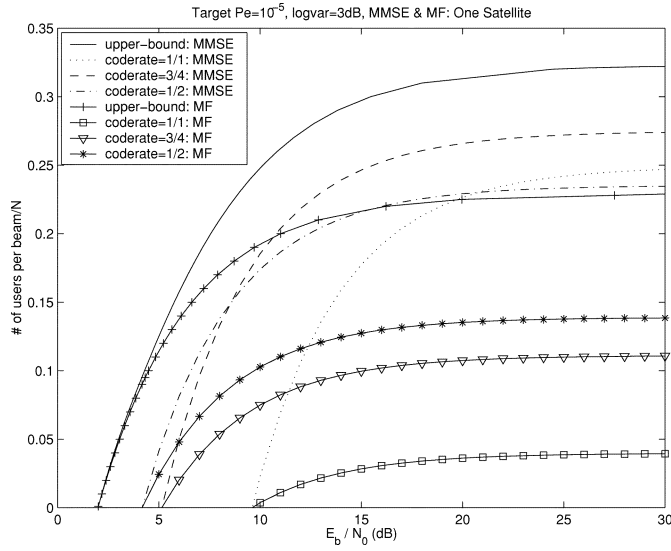


Fig. 13. Comparison of the capacity for different code rates: one satellite.

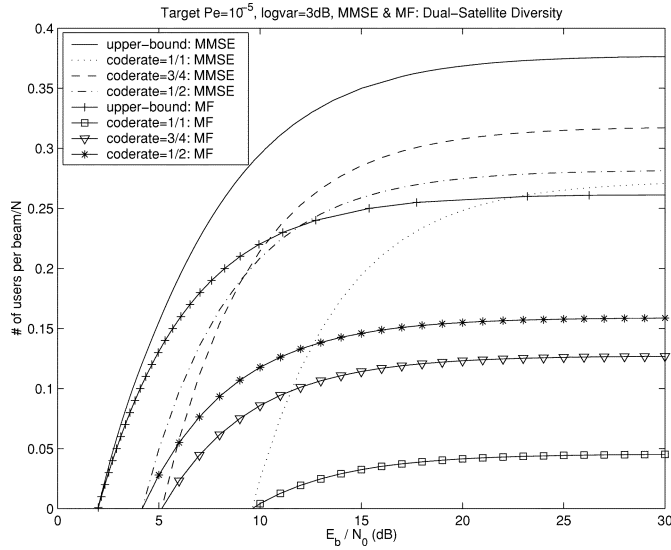


Fig. 14. Comparison of the capacity for different code rates: selective dual-satellite diversity.

over a wide range of loads. Fig. 12 indicates that at a load of 0.25 (32 users/ N) per beam, a rate 1/2 code requires a minimum E_b/N_0 of 7.5 dB for reliable communications.

B. Selection of Code Rate and System Capacity

Figs. 13 and 14 show achievable load versus E_b/N_0 with a single satellite and dual satellite diversity respectively, for the MF and MMSE receivers, and for different code rates. In these figures, the target error rate is 10^{-5} and the standard deviation of the log-normal shadowing is 3 dB. An upper bound obtained from the cutoff rate is also shown in both figures.

To obtain these results, we first compute the target SINR β^* corresponding to the target error rate via the union bound. This depends on the code rate. From (9) and (16) and using the lo-

cation independence assumption, we have $P^r(k_n \rightarrow \mathbf{x}) = P^*(\alpha)Y$, and substituting in (7) gives

$$\alpha = \frac{\frac{P^*(\alpha)}{\sigma^2} - \beta^*}{\beta^* \frac{P^*(\alpha)}{\sigma^2} E \left[\frac{Y}{1+\beta^*Y} \right]} \quad (25)$$

for the MMSE receiver. For the MF, we have

$$\alpha = \frac{\frac{P^*(\alpha)}{\sigma^2} - \beta^*}{\beta^* \frac{P^*(\alpha)}{\sigma^2} E_o [Y]} \quad (26)$$

where $E_o[\cdot]$ denotes the expectation over the user population outside the desired beam. Substituting $\alpha = B(K/RN)$ (total load where B is the number of beams) and $P^*(\alpha)/\sigma^2 = 2R(E_b/N_0)$ in (25) and (26) gives

$$\frac{K}{N} = \frac{2R \frac{E_b}{N_0} - \beta^*}{2B\beta^* \frac{E_b}{N_0} E \left[\frac{Y}{1+\beta^*Y} \right]} \quad (27)$$

for the MMSE receiver and

$$\frac{K}{N} = \frac{2R \frac{E_b}{N_0} - \beta^*}{2B\beta^* \frac{E_b}{N_0} E_o [Y]} \quad (28)$$

for the MF receiver. To compute the upper bound based on cutoff rate, we combine (27) with (24) to obtain

$$\frac{E_b}{N_0} = \frac{\beta^*}{2 \left(1 - \log_2 (1 + e^{-\beta^*/2}) - \frac{KB}{N} E \left[\frac{Y}{1+\beta^*Y} \right] \beta^* \right)}. \quad (29)$$

For fixed load K/N , (29) gives a relation between E_b/N_0 and β^* . The upper bound is then obtained by choosing the minimum E_b/N_0 that satisfies (29).

The results in Figs. 13 and 14 show that for the MF the rate 1/2 code always provides the largest capacity. However, for the MMSE receiver, the optimal code rate depends on E_b/N_0 . In all cases, coding provides a significant increase in capacity at low to moderate E_b/N_0 . These results are consistent with the uncoded results in the preceding section in that the MMSE receiver still offers a capacity gain of 1.5–3 relative to the MF receiver. Furthermore, selective dual-satellite diversity offers a moderate increase in capacity relative to the single satellite case. We observe that the MF benefits much more from coding than the MMSE receiver. This is due to the decrease in spreading gain with coding, which compromises the ability of the MMSE receiver to suppress interference. The upper bound for the MMSE receiver obtained from the cutoff rate is 2–4 dB better than the MMSE performance with finite constraint lengths for $K/N < 0.2$. For large values of E_b/N_0 , the upper bound on load for the MMSE receiver is about 20% higher than the load supported by the codes considered. Comparing the upper bound for the MMSE receiver with that of the MF, these results indicate that with a powerful convolutional code, the relative gain offered by the MMSE receiver is small for low E_b/N_0 . However, for large E_b/N_0 , the MMSE receiver offers a capacity gain of 1.5 relative to the MF receiver.

VIII. CONCLUSION

We have discussed the application of interference-mitigating MMSE receivers to a multibeam, multisatellite CDMA communication system. Our model includes path loss due to the an-

tenna gain pattern, random shadowing, and a one-step power control scheme which makes a single adjustment of transmitted power for each user. A semianalytic method for performance evaluation has been used, which combines the large system analysis of linear CDMA receivers with random codes in [20] with computer simulation to evaluate effective interference. Different methods for power assignment with dual-satellite diversity have also been evaluated.

The analysis and simulation results show that the performance of the MMSE receiver degrades much more gradually than that of the MF receiver as the number of interferers increases. Typical (averaged) capacity gains are in the range of two to three, and the gain is an increasing function of the total power budget per beam, and the variance of the random shadowing. The power control scheme tends to equalize performance over location and shadowing, and decreases the outage probability. With power control the performance variability of the MF receiver is still much greater than that of the MMSE receiver (even when long spreading codes are used with the MF). Transmitter diversity can mitigate the effect of random shadowing, but our results indicate that for the MMSE receiver, only selection diversity gives a performance improvement relative to the single satellite case. This is due to the additional interference added by the second satellite when equal or proportional power control is used.

Our coded results indicate that the MMSE receiver retains its advantage relative to the MF receiver. The optimal code rate for the MMSE receiver depends on E_b/N_0 and the load, although for typical satellite system parameters a rate 1/2 code appears to be close to optimal.

The techniques used here can be applied to other CDMA communications systems, such as terrestrial cellular. For example, a similar type of analysis of an MMSE receiver with one-step power control can be applied with an appropriate modification of channel characteristics.

ACKNOWLEDGMENT

The authors would like to thank R. De Gaudenzi and J. Romero-Garcia for technical discussion concerning this work.

REFERENCES

- [1] F. Adachi, M. Sawahashi, and H. Suda, "Wideband DS-CDMA for next-generation mobile communications systems," *IEEE Commun. Mag.*, vol. 36, pp. 56–69, Nov. 1998.
- [2] E. Dahlman *et al.*, "WCDMA-The radio interface for future mobile multimedia communications," *IEEE Trans. Veh. Technol.*, vol. 47, pp. 1105–1118, Nov. 1998.
- [3] T. Ojanpera and R. Prasad, "An overview of air interface multiple access for IMT-2000/UMTS," *IEEE Commun. Mag.*, vol. 36, pp. 82–95, Nov. 1998.
- [4] M. L. Honig and H. V. Poor, "Adaptive interference mitigation in wireless communications systems," in *Wireless Communications: A Signal Processing Perspective*, H. V. Poor and G. Wornell, Eds. Englewood Cliffs, NJ: Prentice-Hall, 1998.
- [5] R. De Gaudenzi, F. Giannetti, and M. Luise, "Advances in satellite CDMA transmission for mobile and personal communications," *Proc. IEEE*, vol. 84, pp. 18–39, Jan. 1996.
- [6] —, "Design of a low-complexity adaptive interference-mitigating detector for DS/SS receivers in CDMA radio networks," *IEEE Trans. Commun.*, vol. 46, pp. 125–134, Jan. 1998.

- [7] —, "Capacity of a multi-beam, multi-satellite CDMA mobile radio network with interference-mitigating receivers," *IEEE J. Select. Areas Commun.*, vol. 17, no. 2, pp. 204–213, Feb. 1999.
- [8] J. Romero-Garcia, R. De Gaudenzi, F. Giannetti, and M. Luise, "A frequency error resistant blind CDMA detector," *IEEE Trans. Commun.*, vol. 48, no. 7, pp. 1070–1076, July 2000.
- [9] B. R. Vojcic, R. L. Pickholtz, and L. B. Milstein, "Performance of DS-CDMA with imperfect power control operating over a low earth orbiting satellite link," *IEEE J. Select. Areas Commun.*, vol. 12, pp. 560–567, May 1994.
- [10] B. R. Vojcic, L. B. Milstein, and R. L. Pickholtz, "Downlink DS-CDMA performance over a mobile satellite channel," *IEEE Trans. Veh. Technol.*, vol. 45, pp. 551–560, Aug. 1996.
- [11] P. Monsen, "Multiple-access capacity in mobile user satellite systems," *IEEE J. Select. Areas Commun.*, vol. 13, pp. 222–231, Feb. 1995.
- [12] R. De Gaudenzi and F. Giannetti, "DS-CDMA satellite diversity reception for personal satellite communication: Satellite-to-mobile link performance analysis," *IEEE Trans. Veh. Technol.*, vol. 47, pp. 658–672, May 1998.
- [13] J. Romero-Garcia and R. De Gaudenzi, "On antenna design and capacity analysis for the forward link of a multi-beam power controlled satellite CDMA network," *IEEE J. Select. Areas Commun.*, vol. 18, pp. 1230–1244, July 2000.
- [14] E. Biglieri, G. Caire, and G. Taricco, "CDMA system design through asymptotic analysis," *IEEE Trans. Commun.*, vol. 48, pp. 1882–1896, Nov. 2000.
- [15] E. Biglieri, G. Caire, G. Taricco, and E. Viterbo, "How fading affects CDMA: An asymptotic analysis with linear receivers," *IEEE J. Select. Areas Commun.*, vol. 19, pp. 191–201, Feb. 2001.
- [16] W. G. Phoel and M. L. Honig, "Performance of DS-CDMA with pilot-assisted channel estimation and linear interference suppression," in *IEEE Trans. Commun.*, vol. 50, May 2002, pp. 822–832.
- [17] P. S. Kumar and J. Holtzman, "Power control for a spread spectrum system with multiuser receivers," in *Proc. PIMRC'95*, 1995, pp. 955–959.
- [18] S. Ulukus and R. D. Yates, "Adaptive power control and MMSE interference suppression," *ACM Wireless Networks*, vol. 4, pp. 489–496, Nov. 1998.
- [19] M. Honig and W. Veerakachen, "Performance variability of linear multiuser detection for DS-CDMA," in *Proc. IEEE Vehicular Technology Conf.*, Atlanta, GA, May 1996, pp. 372–376.
- [20] D. Tse and S. Hanly, "Linear multiuser receivers: Effective interference, effective bandwidth and user capacity," *IEEE Trans. Inform. Theory*, vol. 45, pp. 641–657, Mar. 1999.
- [21] P. Schramm and R. R. Müller, "Spectral efficiency of CDMA systems with linear MMSE interference suppression," *IEEE Trans. Commun.*, vol. 47, pp. 722–731, May 1999.
- [22] Kiran and D. Tse, "Effective interference and effective bandwidth of linear multiuser receivers in asynchronous systems," *IEEE Trans. Inform. Theory*, vol. 46, pp. 1426–1447, July 2000.
- [23] J. W. Silverstein and Z. D. Bai, "On the empirical distribution of eigenvalues of a class of large dimensional random matrices," *J. Multivariate Anal.*, vol. 54, pp. 175–192, Jan. 1995.
- [24] J. P. Odenwalder, "Optimal Decoding of Convolutional Codes," Ph.D. dissertation, Dept. Syst. Sci., UCLA, 1970.
- [25] J. G. Proakis, *Digital Communications*. New York: McGraw-Hill, 1995.



Weimin Xiao (S'99–M'00) was born in Boyang, China, in 1970. He received the B.S. degree in electrical engineering from Huazhong University of Science and Technology, Wuhan, China, in 1992, the M.S. degree in electrical engineering from Tsinghua University, Beijing, China, in 1994, and the Ph.D. degree in electrical engineering from Northwestern University, Evanston, IL, in 2001.

He is now with Motorola, Inc., Arlington Heights, IL, working on physical layer design for wireless communication networks. His research interests include multiaccess wireless communication, large system performance analysis, adaptive signal process, and radio resource allocation.

Michael L. Honig (S'80–M'81–SM'92–F'97) received the B.S. degree in electrical engineering from Stanford University, Stanford, CA, in 1977, and the M.S. and Ph.D. degrees in electrical engineering from the University of California, Berkeley, in 1978 and 1981, respectively.

He subsequently joined Bell Laboratories in Holmdel, NJ, where he worked on local area networks and voiceband data transmission. In 1983, he joined the Systems Principles Research Division at Bellcore, where he worked on digital subscriber lines and wireless communications. He was a Visiting Lecturer at Princeton University, Princeton, NJ, during the Fall of 1993. Since the Fall of 1994, he has been with Northwestern University, Evanston, IL, where he is a Professor in the Electrical and Computer Engineering Department.

Dr. Honig has served as an editor for Communications for the IEEE TRANSACTIONS ON INFORMATION THEORY, and as an Editor for the IEEE TRANSACTIONS ON COMMUNICATIONS. He has also been a Guest Editor for the *European Transactions on Telecommunications and Wireless Personal Communications*. He has served as a Member of the Digital Signal Processing Technical Committee for the IEEE Signal Processing Society. He is a Member of the Board of Governors for the Information Theory Society.